Materials Advances

ROYAL SOCIETY OF CHEMISTRY

PAPER

View Article Online
View Journal | View Issue

Cite this: *Mater. Adv.*, 2022, 3, 3600

Investigation of interactions between organophosphorus compounds and TiO_2 modified microcantilevers for molecule detection in air†

Urelle Biapo,*[a] Valérie Keller,[a] Philippe Bazin[b] and Thomas Cottineau*[a]

In order to develop a detector working in the gas phase for organophosphorus molecules, resonant microcantilever surfaces were chemically modified with pristine and functionalized TiO_2 nanorods. By using a solvothermal synthesis method a homogeneous film, composed of nanorods with square facets, covering completely the surface of the levers was obtained. The synthesized rods mainly exhibit [110] oriented crystals and this facet has especially demonstrated a high loading ability for grafted sensing molecules. Experimental results showed that the sensing response is three times higher when the TiO_2 sensor is functionalized with amine terminated molecules while no significant response is observed for bare cantilevers exposed to a DMMP simulant. The *in situ* IR analysis highlighted the formation of hydrogen bonds between the characteristic groups of DMMP and the TiO_2 surface at room temperature. The strength of this bond depends on the chemical groups present at the oxide surface. Molecules containing hydroxyl or amino functions form stronger hydrogen interactions with the OP simulant compared to the fluorine group. The kinetics of adsorption are characterized by a fast initial reaction followed by gradual slowing to a steady-state for all the samples.

Received 12th November 2021,
Accepted 7th March 2022

DOI: 10.1039/d1ma01064f

rsc.li/materials-advances

Introduction

The development of efficient and reliable sensors for chemical detection in air is an important applied research area that has a direct impact in monitoring industrial pollution, preventing chemical risks and more generally ensuring public safety providing warnings. Amongst these chemicals organophosphorus (OP) nerve agents are one of the most dangerous chemicals as they are highly toxic to humans even at very low concentrations.[1] Although their main usage in terms of volume is as pesticides, most toxic OP molecules are used as chemical warfare agents. Chemical attacks occurred in Syria and in Japan over the past decade and resulted in several deaths related to these dangerous weapons. Nevertheless, OP pesticides remain the major source of poisoning, especially in developing countries, causing more than 100 000 deaths each year.[2] Therefore, there is an insistent need for a trace level, real-time and on-site detection system of nerve agents in both civilian and military domains. In contrast with the benchmarked techniques (GC-MS, IMS)[3–5] employed to detect this kind of toxic chemical, innovative chemical sensors developed nowadays have the potential to provide a high sensitivity associated with portability and low cost monitoring abilities.[6,7] The working principle of this type of sensor is based on the modification of the intrinsic properties of a chemical layer by the interaction of the target analyte with its surfaces. A microcantilever is a typical chemical sensor platform which has demonstrated ultra-high sensitivity and selectivity towards various types of compounds depending on the coated sensitive layer.[8–10] To reach high sensitivity the resonant frequency of microcantilevers can be tracked using an optical AFM head or using emerging piezoresistive levers which offers opportunities for more compact devices.[11,12] In this case, the active layer is very important because it provides specific adsorption sites necessary to capture the analyte. The selection of an appropriate sensitive layer is usually based on the target analytes and the possible interactions with the sensor surface. This layer is generally made of nanoporous materials, nanostructures,[13] self-assembled monolayers,[14] specific functional molecules, hyper-branched polymers,[15] *etc.* All the cited examples were very promising and showed good responses regarding the detection of volatile organic compounds, moisture or organophosphorus molecules but so far the proposed devices do not fully satisfy all the required criteria in terms of sensitivity, selectivity, rapidity and cost.

[a] *CNRS, Univ. Strasbourg, ICPEES Institut de Chimie et Procédés Pour l'Energie, l'Environnement et la Santé, UMR 7515, 25 rue Becquerel, 67087 Strasbourg, France. E-mail: cottineau@unistra.fr, urelle_biaps@yahoo.fr*

[b] *Normandie Université, ENSICAEN, UNICAEN, CNRS, Laboratoire Catalyse et Spectrochimie, 14050 Caen, France*

† Electronic supplementary information (ESI) available: XPS spectra and data treatment, DMMP detection curves fitting parameters, supplementary TDP with *in situ* IR spectroscopy data. See DOI: 10.1039/d1ma01064f

Besides manufacturing novel sensor technologies which exhibit good performances, it is also important to precisely understand the chemical interactions occurring between the target compounds and the active sensing layer in order to design suitable sensors for toxic or dangerous chemicals. In this context, several studies have focused on understanding the adsorption/desorption mechanisms of OP on different materials. Among them, theoretical studies[16] and solid-state MAS NMR[17] have given interesting results on the adsorption reaction of OP molecules on oxide surfaces such as silica or manganese oxide. An infrared study was used to describe the type of reaction involved for three organophosphorus simulants (MDCP, DMMP, and TCP) on the silicon oxide surface.[18] The results obtained proved that silica is a good candidate for prefiltering and preconcentration strategies which are beneficial in avoiding high false positive results caused by interferent gases. Other materials such as iron oxide, alumina[18] or metal organic frameworks[19] were also investigated using the same technique.

Our team developed different methods to grow TiO_2 nanostructures having a high specific surface area on the microcantilever surface for increasing its active collection area. This concept has been first highlighted in the work described by Spitzer *et al.*, where TiO_2 nanotubes prepared using titanium electrochemical anodization were employed to increase the sensitivity of the cantilever and resulted in a detection limit of 0.8 ppb of trinitrotoluene vapours.[20] This anodization method was improved to increase the surface offered by the TiO_2 nanotubes covering the microcantilever. Furthermore, by achieving nanostructuration on both faces of the cantilever the capture surface and then the sensing performances, were multiplied by a factor of 2.3 for an optical lever entirely covered on both side with TiO_2 nanotubes compared to our initial work.[21,22] As an alternative, a TiO_2 nanostructure can be grown on the optical microcantilever using a versatile solvothermal route. This low temperature method is more compatible with small silicon substrates than chemical anodization which requires fluoride ions in the electrolyte and deposition of a thick layer of titanium ($\sim$5 μm).[23,24] The TiO_2 nanostructure obtained by solvothermal synthesis exhibits a higher surface area than the NTs obtained by anodization and we demonstrated that its interaction with the analyte molecules can be further improved by grafting oxime terminated molecules that could selectively bind to the OP analyte.

In the present study, we report the influence of different sensing groups on detecting nerve agents in the gas phase and the interactions involved with nanostructures created at the surface of such microcantilevers. Three types of molecules were used to functionalize the TiO_2 nanostructured surfaces. They have a similar architecture including an aromatic spacer and a carboxylic acid tethering group but differ in their terminal groups (oxime, amine or fluorine functional group as depicted in Scheme 1) which play the role of active sites for OP simulant absorption. A detailed characterisation of the nanostructure and the functionalized sample is presented, with particular attention on the evidence of the grafting process at the TiO_2 surface. The detection tests were carried out on dimethyl methylphosphonate (DMMP), a common OP simulant. Since little is known about the molecular interactions between DMMP and functionalized TiO_2, after investigating the performance of the sensors, specific *in situ* analysis was performed using infrared spectroscopy to determine the reaction mechanisms involved when the organophosphorus agent is in contact with the modified surfaces.

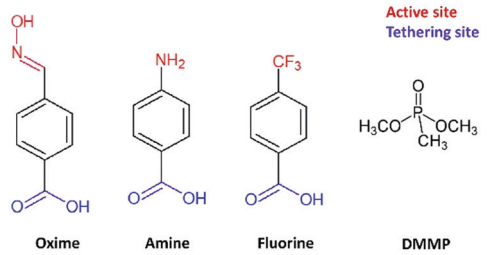

Scheme 1 Chemical structures of the molecules used for the functionalization of the nanostructured microcantilever and of the OP simulant (DMMP).

Experimental

Sensor preparation

Commercial silicon microcantilevers (TL-NCL-50 tipless type; NanoSensors™) were employed in these experiments. Their resonant frequency is in the range of 146–236 kHz and their nominal dimensions are 7 μm in thickness, 225 μm in length, and 38 μm in width. A deposition of 50 nm of metallic titanium by DC magnetron sputtering (Fig. 1, Step a) followed by a heat treatment (Step b) was used to coat a seed layer on the cantilever surface. The detailed conditions for the preparation of this layer, required to initiate the growth of the TiO_2 nanostructure, have been described elsewhere.[23] The modified lever was then nanostructured by the solvothermal method in an acidic medium (Step c). In a typical synthesis, 15 mL of hydrochloric acid (37%, Acros Organics) and 15 mL of ethanol (98%) were mixed and stirred for 5 min. Then, 0.5 mL of titanium isopropoxide (TTIP, 97%, Sigma Aldrich) was added to the mixture as the TiO_2 precursor. The final solution was poured into a Teflon vessel placed in a stainless-steel autoclave and kept under solvothermal conditions at 150 °C for 8 hours. After the synthesis, the obtained sensors were rinsed successively with ethanol and acetone in order to remove any residual chemicals and poorly attached nanoparticles.

The IUPAC nomenclature of the molecules used for surface functionalization is (*E*)-4-((hydroxyimino)) methyl benzoic acid, 4-aminobenzoic acid and 4-trifluoromethyl benzoic acid and they are denoted, respectively, as oxime, amine and fluorine in the manuscript. The oxime molecule was synthesized as

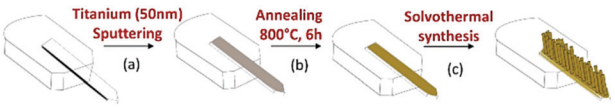

Fig. 1 Nanostructuration of cantilevers with TiO_2.

described previously in the literature[25] while amine, fluorine and DMMP molecules were purchased from Sigma Aldrich and used without further purification. To modify the nanostructured cantilever surface, a 0.01 mol L^{-1} solution of the oxime, amine or fluorine molecules was prepared in a mixture of acetonitrile and *tert*-butanol in a volumetric proportion of 1 : 1. The nanostructured sensor was dipped and kept for 24 hours in the solution at 70 °C.

Gas phase detection of OP

The modified optical cantilever was installed in a PicoSPM multimode AFM in the dynamic mode to activate vibration and record the resonance frequency shift of the lever. For the detection tests, the nanostructured and functionalized cantilevers were inserted into a lab-made chamber in which the atmosphere can be control by flowing different gases mixtures. This system allows adjusting the vapour concentration of DMMP, and by using a GC-MS analyser (model 7890A-5975, Agilent) connected to the exit of the chamber the DMMP was measured at 105 ± 6 ppm for all the analysis. The chamber and gas line were maintained at 30 °C to avoid DMMP condensation. Before each test, the cantilever was allowed to stabilize for 30 minutes under a clean air flow to reach a constant frequency (f_0) which serves as the baseline. A 4-way valve allows switching between the reference air and the DMMP containing air during measurements with a constant flow of 50 mL min^{-1}. For each test, the cantilever was exposed to DMMP vapour for 10 minutes and its resonance frequency (f) was followed as a function of time during absorption and desorption. The recorded frequency change Δf represents the sensing response.

Characterization

The morphology of TiO_2 nanostructure was investigated by scanning (SEM; JEOL JSM-6700F FEG) and transmission (TEM; JEOL 2100F TEM/STEM) electron microscopies. The Raman spectra of the samples were obtained in the spectral range of 50–3000 cm^{-1} using a Raman spectrometer (Horiba Jobin Yvon; Aramis) with a laser excitation wavelength of 532 nm. Fourier transform infra-red (FT-IR) spectroscopy was used to investigate the interaction between functionalized TiO_2 and the target compound. The spectra were collected using a Thermo Nicolet NEXUS 670 spectrometer equipped with a MCT detector. A Thermo VG Scientific equipment was used to conduct X-ray photo-electron spectroscopy (XPS) analysis. Recorded data were processed with CasaXPS software and the spectra were corrected using the adventitious carbon peak (284.9 eV) as the internal energy reference for all the samples. UV-vis spectroscopy was carried out using a PerkinElmer Lambda 950 spectrometer in the region of 200–400 nm.

In situ infrared measurement

A commercial TiO_2 powder (UV100-Hombikat, Sachtleben Chemie GmBH) was functionalized under the same conditions as the nanostructured cantilevers to verify the grafting process and for *in situ* analysis. 150 mg of the powder was introduced into the solution containing the molecules to be attached. After the 24 h of reaction, TiO_2 particles were first separated from the solution by vacuum filtration, and then, rinsed several times with acetone and ethanol to remove the solvent as well as the non-attached molecules. The samples were finally dried at room temperature overnight.

In this study, *in situ* FT-IR analyses were conducted in a home-made IR cell recently developed in the LCS laboratory for adsorption experiments. This cell called ''Jumpipe'' is connected to a pumping system for the treatment under vacuum of the sample ($<10^{-5}$ torr) and for probe molecule addition. Briefly, the shape of the main part of the cell is a cylinder made of quartz that carries a 2-position sample holder in its center (a position for the gas phase or the background acquisition and a position for the sample). The functionalized TiO_2 powder was pressed into a pellet with a diameter of 13 mm to be used in the experiments. The heating system surrounding the quartz tube can reach 500 °C, whereas an air cooling system protects the two terminal KBr windows. Taking into account the configuration of the Jumpipe cell, the sample is always maintained at the temperature of the oven (no return to room temperature for the acquisition of the IR spectrum). Usually for IR experiments, the pellets were first, treated under vacuum ($<10^{-5}$ torr) at 25 °C and then, exposed to 0.3 torr eq.$^{-1}$ of DMMP at room temperature until the saturation of the surface is observed. After taking the spectra of the adsorbed DMMP, the oxide samples were exposed again to a vacuum of 10^{-5} torr for 15 minutes and then heated from 20 to 300 °C at a heating rate of 5 °C min^{-1}. The temperature of 300 °C was maintained for 15 min, followed by the cooling of the sample to room temperature. IR spectra (64 averaged scans per spectrum) were collected in the transmission mode every minute with a resolution of 4 cm^{-1} during the entire analysis using a Thermo Nicolet NEXUS 670 spectrometer, equipped with a MCT detector.

Results and discussion

After solvothermal synthesis, a film can be optically observed on the silicon cantilever. Fig. 2 displays the structural and morphological characterization performed on the nanostructured cantilever. A well-organized layer of TiO_2 nanorods (NRs) is uniformly distributed at the silicon cantilever surface, as observed in the SEM images (Fig. 2b, top and cross-sectional views). The top of the film is made up of small square facets of the nanorods having a width of 15 nm and their length is approximately 2.5 μm. Thanks to the small diameter of the green laser spot used in Raman spectroscopy, the crystalline structure of TiO_2 could be determined directly on the cantilever surface. Three Raman peaks visible at 609, 430 and 230 cm^{-1} are respectively assigned to the A_{1g}, E_g and multiple phonon scattering of the rutile TiO_2 phase[26] (Fig. 3a). Silicon peaks are also evidenced on the Raman spectra. Uncovered silicon substrates as well as a commercial rutile powder were also analysed by Raman spectroscopy as references. All the peaks from both references appeared in the Raman spectrum of the nanostructured cantilever and no new contribution appears. This formation of rutile is in accordance with our

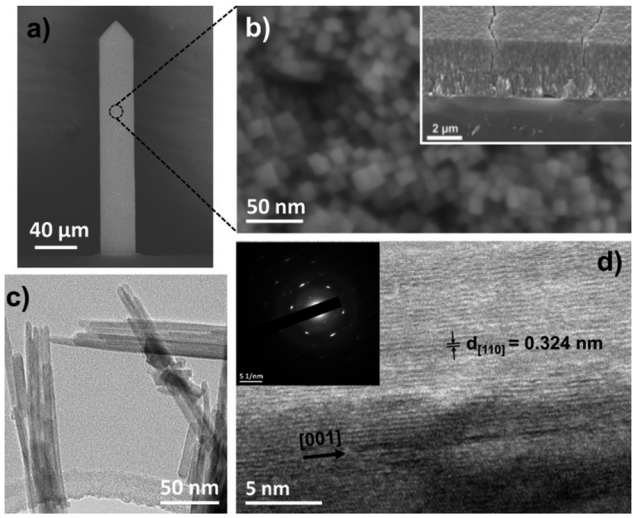

Fig. 2 (a) SEM images of a nanostructured cantilever. (b) Top and cross-sectional (inset) SEM images of rutile TiO_2 NRs. TEM images of single rutile TiO_2 nanorod (c) at low and (d) high magnification.

previous observations by XRD and Raman analysis for TiO_2-NRs grown using the same synthesis route on a centimetric silicon substrate.[23]

The presence of the rutile crystalline structure of TiO_2 only, is highlighted in the TEM image and SAED. Furthermore, as shown in Fig. 2d, the nanorods are monocrystalline with their lateral faces being composed of (110) crystal planes according to the measured interplane distance (d_{110} = 0.334 nm) and the preferential growth direction is along the [001] axis.[27] This morphology is explained by the presence of chloride ions which are known to promote the anisotropic growth of TiO_2.[26,28,29]

A commercial TiO_2 powder was used in order to validate and study the grafting process of the different molecules on the surface. An important parameter to achieve reliable measurements is the density of the grafted groups. The synthesized nanostructure has a high surface area of around 250 m^2 g^{-1}. Commercial or synthesized rutile powders have a limited surface area (<10 m^2 g^{-1}) due to large crystallite and particle size. Consequently the grafting density is low and the resulting IR signal too weak for *in situ* IR analysis. For this reason, even if it is mainly anatase, we choose the Hombikat UV100 powder because of its higher specific surface (250 m^2 g^{-1}) comparable to that of the nanorod film. Furthermore this TiO_2 powder is known to have a significant amount of amorphous phase with high Ti–OH density that offers numerous grafting sites. The molecules were grafted at the surface of the particles as described in the experimental part and then analysed by infrared spectroscopy. Fig. 3b shows the FT-IR spectra (recorded after vacuum reached $P < 1 \times 10^{-5}$ mbar at room temperature) of the pristine TiO_2 anatase and also the powder modified with the three molecules. Bands below 1000 cm^{-1} observed for all the samples correspond to the stretching vibration of the Ti–O–Ti bonds.[30] On the bare TiO_2 sample, the bands at 3700–3600 cm^{-1}, 3500–3000 cm^{-1} (broad) and 1625 cm^{-1} are due to vibrations of isolated OH-groups, OH-groups which are H-bonded with adsorbed water molecules and water molecule deformation ($\delta(H_2O)$), respectively.[30–33] All the modified samples showed the presence of symmetric and antisymmetric vibrations of carboxylate group around 1415 and 1510 cm^{-1}. The split between the two carboxylate peaks suggests a bidentate association[34,35] at the TiO_2 surface and clearly confirms the presence of the molecules on the oxide. Furthermore, this bidendate configuration is also supported by the absence of any peak characteristic of carbonyl function of carboxylic acid around 1700 cm^{-1}. This also suggests that the weakly bonded molecules were efficiently removed during the cleaning procedure.

Typical peaks for each molecule are also observed by IR, shown in Fig. 3b. For instance, the ν(C=N) band for the

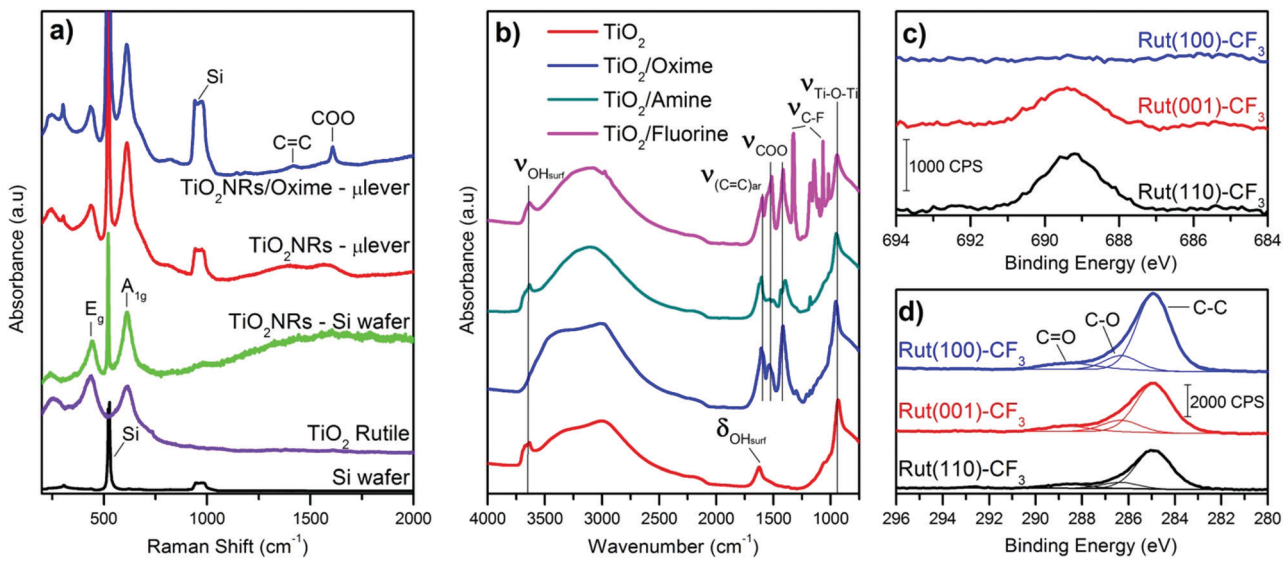

Fig. 3 (a) Raman spectra of the nanostructured cantilever, a silicon bare and a commercial rutile powder. (b) IR spectra of TiO_2 and functionalized TiO_2. XPS analysis showing the (c) F 1s peaks and (d) C 1s peaks of monocrystals functionalized with fluorine molecules.

TiO_2–oxime (1650 cm^{-1}) and the δ(N–H) of TiO_2–amine (1627 cm^{-1}) appear as a shoulder of the $\nu(C{=}C)_{ar}$ band at 1600 cm^{-1}. In the case of the fluorine modified surface, several thin peaks between 1000 and 1350 cm^{-1} are attributed to the stretching band of C–F. The presence of both broad bands around 3500–3000 cm^{-1} and at $\approx$1625 cm^{-1} (shoulder) shows that residual water remains adsorbed on the TiO_2 modified samples. Note that $\delta(H_2O)$ is generally of low intensity and hidden by the bands of the additives molecules also present in this spectral region. These results further indicate the effectiveness of the modification of the surface of anatase particles by the aromatic sensing molecules.

Based on these analyses and proof of concept realized with powdered TiO_2, the nanostructured microcantilevers were also functionalized with the 3 types of molecules. Since it is not possible to perform FT-IR or XPS for the lever due to its brittleness and small size, we analysed the modified sensor by Raman spectroscopy. The spectrum was collected before and after the grafting process. Beside the peaks attributed to the oxide, two new peaks related to carboxylate (COO) and carbon double bond (C=C) are found and clearly depict the presence of molecules on the TiO_2–cantilever (Fig. 3a). This characterisation indicates that the sensing film combining high surface by TiO_2 nanorods and immobilized functional groups has been successfully prepared on microcantilevers.

TEM and electron diffraction indicate that the rutile nanorods grow in the *c* direction with (001) facets on the top and (110) crystal planes constituting the side of the rods. In our previous work, we demonstrate by EDX that despite the high compactness of the nanostructure film, fluorine is present in the whole thickness of the fluorine modified nanorod film (from the top to the bottom) confirming the efficiency of the grafting. In order to investigate more in detail the interaction between the organic molecule and the different crystal facets of the nanorods, three rutile monocrystals ((110), (001) and (100) crystal orientation) were functionalized under the same conditions as those of the powder and microcantilever. The modified single crystals were characterized using XPS because no signals from the grafted molecules were detected by FT-IR or Raman spectroscopy due to low surface and consequently low molecular density. For these XPS analyses of functionalized monocrystals, we selected only the fluorinated molecules because it is easier to identify fluorine atoms compared to C, N and O atoms which compose the oxime or amine molecules and are also naturally present at the surface of TiO_2 as adsorbed moieties. Obviously, the titanium (Ti $2p_{1/2}$ and Ti $2p_{3/2}$) and oxygen (O 1s) peaks were identified on the modified monocrystals surfaces and are characteristic of TiO_2 (ESI,† Fig. S1 and Table S1). As depicted in Fig. 3c, the fluorine (F 1s) peak is visible only for the (110) and (001) crystal surfaces. Its binding energy identified at 687.3 eV corresponds to the fluorine element attached to carbon.[36] Quantitative analysis shows that, the F/Ti ratio is similar for the (110) and (001) facets while it is almost zero for the (100) one. Additionally, a small peak at 292.4 eV assigned to carbon involved in a C–F bond is only observed for this (110) facet, shown in Fig. S1b (ESI†). This result indicates the high proportion of fluorine molecule adsorbed on this crystal surface. We can conclude that the (110) and the (001) rutile surfaces possess a higher number of active sites for the chemical anchoring of the organic molecules while no significant grafting is observed on the (100) surface. This result is important with regards to our aimed application and explains why grafting is effective since the synthesized rutile TiO_2 nanorods mainly exhibit the (110) crystal facet and (001) to a less extent at their terminating surface.

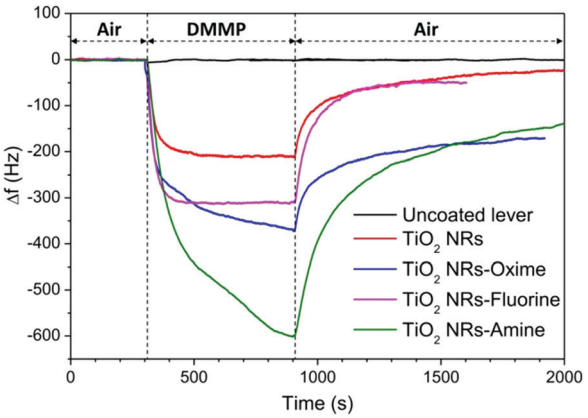

Fig. 4 Sensing response of nanostructured and functionalized cantilevers exposed to 105 ppm of DMMP vapour at 30 °C.

The resonance frequency changes of TiO_2-nanostructured and functionalized microcantilevers towards exposure to DMMP are shown in Fig. 4. The measurement cycle is after 5 min of exposure of the sensor to clean air, followed by 10 min of DMMP vapour generation in the detection chamber and back to clean air. For the pristine cantilever, the resonance frequency remained unchanged during the generation of the simulant in the detection chamber indicating no significant response to DMMP vapour of this lever. This result is due to the low surface area of the silicon surface and to the weak affinity between silicon and the target gas. For the other sensors, the resonance frequency significantly drops when the cantilever surface is nanostructured and/or chemically modified and the response significantly changes depending on the layer covering the lever. Due to its high capture surface, the presence of TiO_2 nanostructure alone strongly increases the frequency shift of the lever exposed to DMMP. A response $\Delta f = -210$ Hz is measured for this sensor. A return to the initial resonance frequency is observed once the DMMP loaded atmosphere is replaced by the reference air, but the cantilever does not immediately return to its baseline after the flow of clean air. This can be due to DMMP molecules that remain attached to the nanorod surface and to the fact that the complete desorption and diffusion is slow in the compact TiO_2 nanostructure as highlighted in a previous study.[23]

The responses of the functionalized samples are always more important than those of the nanostructured one. Two combined effects could explain this higher sensitivity of the functionalized lever: the large loading ability of the nanostructure combined with the high reactivity of the functional groups towards the organophosphorus agent. Frequency shifts of −312 Hz, −372 Hz and −604 Hz are measured for fluorine, oxime

Table 1 Sensing properties of the nanostructured and functionalized cantilevers

Sample	n (nmol cm^{-2})	$\Delta f_{10\,min}$ (Hz)	t_{ads} (s)	t_{des} (s)
TiO_2	—	−210 ± 15	103.1	419.2
TiO_2–fluorine	113	−312 ± 15	30.8	118.9
TiO_2–oxime	133	−372 ± 15	235.5	352.7
TiO_2–amine	205	−604 ± 15	238.0	499.7

and amine modified sensors, respectively (see Table 1). The fluorine functionalized cantilever exhibits the weakest response among the three sensors whereas the highest Δf is obtained for the amine functionalized sensor. The frequency shift as a function of time during adsorption and desorption steps was fitted using exponential functions (see ESI† Fig. S2) and time constants related to adsorption and desorption (t_{ads}; t_{des}) mechanisms were determined (Table 1). Table 1 shows that DMMP is adsorbed twice as slowly on levers functionalized with molecules having a nucleophilic group (oxime) or function that provide hydrogen bonds (amine) than on the simply nanostructured lever. These differences may be explained by the different chemical structures of the grafted moieties. The hydrogen of $-NH_2$ as well as the nucleophilic oxime (–N═OH) terminal groups can form hydrogen bonds with the P═O group of the DMMP, whereas the $-CF_3$ groups are hydrogen bond acceptors that can establish weak hydrogen bonds with the $-O-CH_3$ of DMMP (<15 kJ mol^{-1}).[37] Furthermore, the amine group is closer to the aromatic group in comparison with the oxime group. In this configuration, a good electronic communication between the tethering site and the active site is favoured and probably influences the strength of the hydrogen bonds involved.

It has also been reported that the oxime group might undergo a nucleophilic substitution reaction with the electrophilic phosphorous site and form a covalent bond between the DMMP and the oxime molecule that is used in the OP intoxication treatment.[38] This assumption might explain the longer recovery rate and the limited desorption of DMMP from the surface of the oxime functionalized cantilever during exposure to blank air.

Another factor to take into account is the grafting ability of the functional molecules. This value was evaluated by UV visible spectroscopy after desorption following a procedure detailed in our previous work. The results indicate a higher density of grafted molecules per surface of TiO_2 (column n in Table 1) for the amine molecule (205 nmol cm^{-2}) than for oxime (133 nmol cm^{-2}) or fluorinated molecules (113 nmol cm^{-2}). These values might also explain the difference in adsorption since the ratio between n and Δf is a constant of 0.35 ± 0.01. Concerning the fluorine modified sensor, a different adsorption mechanism might occur considering the lower time constant (t_{ads} = 30.8 s) obtained while the target molecule is adsorbed. The desorption rate seems also to depend on the type of functional group present at the sensor surface. It occurs more slowly for the levers having –OH or $-NH_2$ terminal groups in comparison with $-CF_3$. Furthermore, for the later the resonant frequency seems to return faster to its baseline. Based on these observations, we believe that the fluorine sensor form weaker interactions with DMMP which results in lower sensitivity but faster response and recyclability of the sensor.

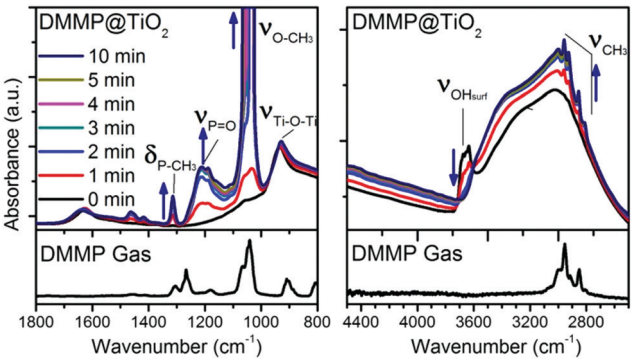

Fig. 5 Infrared *in situ* study showing the adsorption of DMMP on pristine TiO_2 powder in the low and high wavenumber of the IR domain. The bottom part represents the spectra of free DMMP in the gas phase.

In order to investigate more in detail the reaction mechanisms involved between the organophosphorus molecules (DMMP) and the different sensing surfaces (TiO_2 powder and functionalized TiO_2 powder), an *in situ* infrared study was conducted. Before introducing the DMMP vapour into the cell, the FT-IR spectrum of the TiO_2 powder was obtained under vacuum as the starting point (black spectrum for t = 0 min in Fig. 5). For comparison the spectrum of DMMP in the gas phase is presented (bottom part of Fig. 5). As shown in the low frequency region of IR spectra (Fig. 5, left), there are several peaks characteristic of the DMMP molecule which appear in the first minute of exposure of the TiO_2 sample to the DMMP molecules. For instance, the peak around 1213 cm^{-1} is attributed to the stretching vibration of the P═O group and the peak at 1315 cm^{-1} corresponds to the deformation band δ_s(P–CH_3) of the DMMP molecule.[39] The split bands located at 1033 and 1067 cm^{-1} correspond to the methoxy ν(O–CH_3) contribution.[40] In the high frequency region, the 4 methyl scissoring vibrations of DMMP are evidenced between 2965 and 2813 cm^{-1} (Fig. 5, right).

The intensity of the DMMP peaks significantly increases with time whereas a diminution of the band corresponding to the free –OH from the titanium dioxide surface is observed (3600 cm^{-1}). All the free –OH groups are consumed when the surface is saturated which seems to occurs in less than 5 minutes according to the spectra in Fig. 5, right. This result highlights the implication of the –OH functional groups at the surface of TiO_2 in the reaction with OP molecules.

By comparing the IR patterns of DMMP in the gas phase with the adsorbed DMMP, the only significant shift is observed for the ν(P═O) vibration (53 cm^{-1}), thereby indicating that the adsorption of molecules might involve this phosphorous oxygen bond as already observed in MoO_3.[40] In summary, the presence of all the typical DMMP bands suggests its molecular adsorption at the TiO_2 surface by the formation of hydrogen bonds between the surface hydroxyl functions and the P═O group, as mentioned in the literature.[18]

In the case of functionalized samples exposed to the target gas, we observed IR bands relative to each grafted molecule as

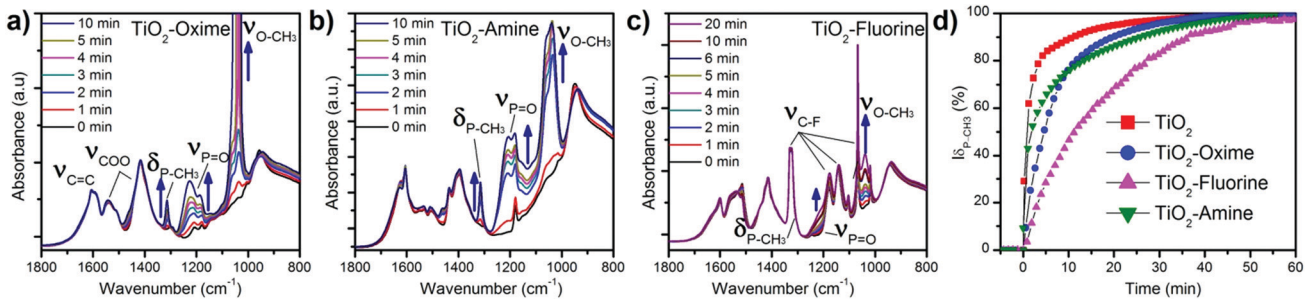

Fig. 6 Infrared analysis showing the adsorption of DMMP on functionalized TiO_2 powder. (a) TiO_2–oxime (b) TiO_2–amine and (c) TiO_2–fluorine. (d) Evolution of the P–CH_3 band area during the adsorption of DMMP (ν(P═O) in the case of TiO_2–fluorine).

well as peaks corresponding to the adsorption of DMMP already observed in the case of the TiO_2 surface (Fig. 6a–c). The three main peaks (νP═O, δ_sP–CH_3, and νO–CH_3) of DMMP increase with exposure time. We noticed a similar DMMP peak evolution for TiO_2–oxime and TiO_2–amine which means that the reaction mechanism involved seems to be very close (Fig. 6a and b). As for the pristine TiO_2, only the phosphorous site ν(P═O) exhibits a high frequency shift of 41 and 58 cm^{-1}, respectively, for TiO_2–oxime and TiO_2–amine in comparison with the DMMP gas. The DMMP is probably adsorbed on these two samples *via* the P═O group through hydrogen bond formation with the outer layer which is composed of amine group or hydroxyl terminal groups (known as two strong hydrogen bond donors). Nevertheless, the presence of adsorbed DMMP on the surface does not induce any significant shift of the oxime or amine group vibration frequencies.

In contrast, the TiO_2–CF_3 sample does not behave like the other functionalized TiO_2. Among the DMMP bands, at first sight only ν(O–CH_3) is clearly visible on the spectra, indicating a modification in the chemical environment of this sample. In comparison with the spectra shown in Fig. 6a and b, only a slight bump is observed around 1240 cm^{-1} which suggests the presence of the ν(P═O) group (Fig. 6c). For this sample, the δ(P–CH_3) band of DMMP is barely visible in Fig. 6c as a shoulder at the right of the intense ν(C–F) band which absorb in the same domain. Considering the lowest intensity of the ν(O–CH_3) band in this case (relatively to νCOO) and the smaller shift of the ν(P═O) band, it can be assumed that the interactions between DMMP and TiO_2–CF_3 are different and probably weaker than for other functionalized TiO_2 samples, as suggested by detection results. This result could explain why the recovery rate of the TiO_2–CF_3 functionalized cantilever is faster. TiO_2–amine and TiO_2–oxime seem to form stronger hydrogen bonds with DMMP which are more stable during the desorption process. The area of the δ(P–CH_3) band is presented in Fig. 6d (normalized to the value of saturation). For the fluorine sample, we used the ν(P═O) vibration at $\sim$1210 cm^{-1} considering that the δ(P–CH_3) peak is hidden beside the ν(C–F) peak. The area of the DMMP characteristic band increases rapidly when the DMMP gas is introduced into the cell. The areas of this peak reach 47, 76, 78 and 89% of its maximum value after 10 minutes of exposure for TiO_2–fluorine, TiO_2–amine, TiO_2–oxime and TiO_2, respectively, confirming that the time required to achieve saturation of the surface depends on the grafted molecule. Similar to our observations during detection tests, the adsorption on TiO_2 surface is faster than for the oxime and fluorine modified surfaces. For fluorine the results differ from our previous observation since it is now a slower sample but it must be reminded that for the analysis of this sample a different peak was used for the kinetics (ν(P═O) instead of δ(P–CH_3)). Furthermore, conditions for *in situ* IR differ from the analysis on microcantilever in the AFM dynamic mode (partial vacuum *vs.* air flow, powder pellets *vs.* microcantilever).

To further understand the surface reaction mechanisms and in the perspective of the use of this type of gravimetric sensor under real conditions, we also examined the influence of relative humidity during the adsorption of DMMP on the functionalized oxide surface. Indeed several studies reported various effect of the presence of water on the absorption of DMMP by oxide materials,[41,42] and a recent study highlighted that the influence of water differs from one material to another.[43] In our experiments, a vapour pressure of 1 torr eq.$^{-1}$ of water (approximately RH = 5%) was introduced in the cell for 10 minutes before exposing the sample to DMMP gas. This experiment was performed on TiO_2–oxime since it presented a significant intensity of δ(P–CH_3) and the area of this peak was plotted as a function of time for investigation. In the presence of water, a slow increase of the typical bands of the DMMP molecule is observed upon exposure of the sample to the simulant (Fig. 7a). Under these conditions the peaks never

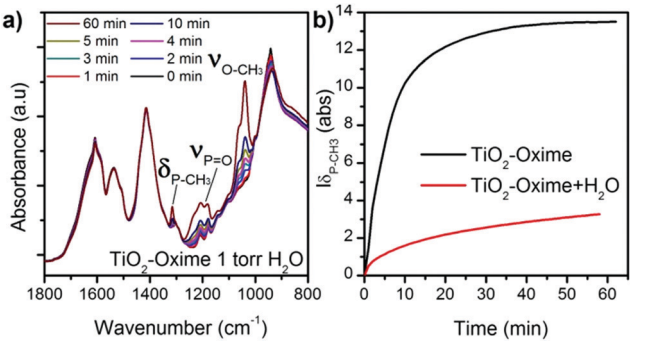

Fig. 7 (a) IR patterns of TiO_2–oxime collected in the presence of humidity, and (b) evolution of the P–CH_3 band area during the adsorption of DMMP with and without water in the chamber atmosphere.

reach saturation, as was observed in the absence of humidity. Moreover, as shown in Fig. 7a, all the peaks attributed to DMMP are less intense (relative to the peaks of νCOO from the oxime molecule) compared to those of the sample without water exposure reported in Fig. 6a. These results suggest a competition between the water and the DMMP molecules which significantly influences the kinetic of adsorption and the amount of adsorbed DMMP at the surface or that water molecules are involved in a hydrolysis process that limits the interactions between DMMP and the oxime nucleophilic group.[41]

The *in situ* analysis showed that, after being exposed to DMMP and then to high vacuum without water traces, DMMP remained strongly attached to the sample regardless of the sensing layer nature. This result is different from the one observed regarding the exposure of modified cantilevers to DMMP. In the sensing experiments, DMMP is desorbed from the surface when a flux of clean air is introduced into the detection chamber. During the *in situ* analysis, the sample is under high vacuum while in the DMMP testing chamber the microcantilever is exposed to a gas flow containing 3 ppm of water vapour. The presence of this residual water may help to desorb the target gas molecule from the surface in sensing experiments.

To observe the influence of relative humidity under more realistic conditions, ATR IR experiments were conducted *ex situ* on a silicon wafer nanostructurated with the same rutile TiO_2–NRs as obtained on the microcantilever. We exposed this sample to concentrated DMMP vapor and then at $t = 0$ put it in ambient air (50–70% RH). We recorded IR ATR spectra at 0, 5 and 10 min after exposure (Fig. S5, ESI†). A $t = 0$ we observed a strong signal of DMMP confirming its absorption on the TiO_2 nanostructure. This signal decreases with exposure to air but is still visible after 5 min. This supplementary experiment confirms that water molecules allow desorbing DMMP and allow recovering the nanostructure surface while the relative humidity does not prevent the initial DMMP absorption.

As described previously, ambient temperature and vacuum are not enough to remove DMMP from the oxide surface in the perspective of regenerate the sensor. A thermal programmed desorption (TPD) associated with IR acquisition over time was performed to get information about the desorption mechanisms of the simulant from the bare and modified TiO_2. The sample in the IR cell was heated at 5 °C min^{-1} from 20 to 300 °C under high vacuum. The infrared spectra of titania powder after its exposure to DMMP were collected at different temperatures and are presented in Fig. 8. Some of the bands attributed to DMMP (such as O–CH_3 or P═O) decrease and finally disappear as the temperature increases. In contrast, the intensity of P–CH_3 around 1314 cm^{-1} remains constant despite the heating. In the region of CH_3 stretching around 3000 cm^{-1} a similar effect is observed: the peak attributed to symmetric and asymmetric ν(O–CH_3) disappears while the doublet of ν(CH_3) stays visible at 2926 & 3000 cm^{-1}. At the same time, a new absorption peak appears at 1110 cm^{-1}, attributed to ν(O–P–O) which is certainly due to the formation of a bond within the metal oxide surface (–P–O–Ti). The formation of this

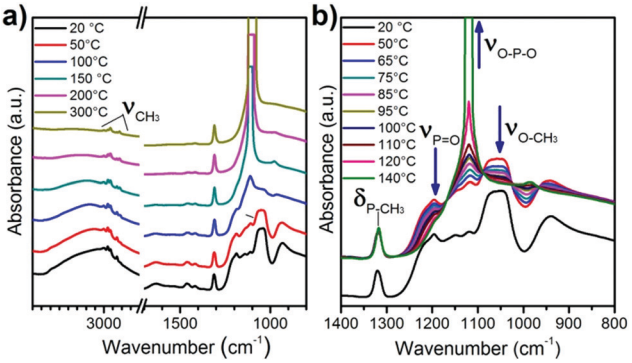

Fig. 8 IR patterns of TiO_2 recorded during the thermal programmed desorption (a) between 20 and 300 °C and (b) magnification of the spectra obtained between 20 and 140 °C.

chemical group might result from the reaction of the P═O function with the surface OH groups and the elimination of the methoxy groups to form methanol. This can also be visualized by the decrease of the broad band around 3200 cm^{-1} associated with adsorbed water and hydroxyl groups. Based on these observations, we conclude that the temperature increase allows a dissociative adsorption of DMMP at the oxide surface. The formation of a strong covalent bond was already observed by TPD on oxide materials such as WO_3, TiO_2 or MgO with organophosphorus molecules.[18] Nevertheless, during our detection experiments at room temperature on microcantilevers, this process does not seem to occur since the resonant frequency returns close to its initial value during desorption. In this case, the aforementioned mechanism involving water molecule is more likely to occur since residual water can be present in the air flow used during DMMP absorption experiments.

In the case of functionalized TiO_2 powders, during heating, the ν(P═O) and the ν(O–CH_3) of DMMP were also evidenced and disappear during the thermal desorption (ESI† Fig. S3 and S4). For the oxime these peaks disappear totally at 200 °C while for the fluorine modified sample at 150 °C it is not visible suggesting again a weaker interaction between the DMMP and the fluorine molecule than the other surfaces. The δ(P–CH_3) band is visible for the oxime modified sample and decreases between 20 and 150 °C but does not disappear completely and a shoulder appears around 1100 cm^{-1} in the same area as the ν(O–P–O) observed during DMMP desorption for the TiO_2 surface. This last observation suggests that a part of DMMP is removed by thermal desorption, but some molecules are removed by the dissociative mechanism observed on TiO_2, presumably by involving the –OH group of oxide uncovered by the grafted molecules. In the case of fluorine modified samples, this mechanism cannot be observed due to the overlap of δ(P–CH_3) and ν(O–P–O) with ν(CF_3) still available after the grafting.

Finally these results also bring important information about the stability of the grafted molecules towards temperature. Indeed if the peaks of the carboxylate function are still visible until 300 °C and do not seem affected until 300 °C, the

vibrations attributed to $\nu(CF_3)$ between 1000 and 1200 cm^{-1} are modified with the temperature increase and some of them disappear totally at 200 °C.

Conclusions

In this work we aimed to gain some fundamental knowledge on the parameters that can improve the sensing layer of a micromechanical sensor for OP detection. Microcantilevers were covered with a homogeneous TiO_2 nanostructure offering a high surface area for molecule capture. These sensors were functionalised with molecules bearing different terminal groups for which different reactivities toward OP are expected.

In order to precisely investigate the grafting process of the molecules on the TiO_2 surface, infra-red, Raman and XPS techniques were employed. The molecules are adsorbed on TiO_2 through carboxylate groups in a bidentate association and from XPS analysis on TiO_2 rutile monocrystals, we identify the (110) and (001) faces as the most efficient for the grafting process. This result is important since TEM electron diffraction indicates that TiO_2 NRs mainly have exposed (110) crystal facets. The fabricated microcantilever sensor covered with the nanostructure and the different molecules was tested for the detection of DMMP. all of the functionalized levers present a higher response than the TiO_2 nanostructure alone. We attempt to explain the difference of response in terms of interaction *via* hydrogen bonds. Amine and oxime terminated molecules are hydrogen donors that present a higher bond energy than fluorine groups (acceptor), which results in higher sensitivity but slower response time and recovery.

To further study this mechanism *in situ* DMMP adsorption on TiO_2 powder was conducted in an IR chamber. The results indicate that in the case of TiO_2 the interaction occurs between the oxide surface and the target molecules through the formation of hydrogen bonds between the surface OH and P═O bond of the DMMP. In the case of amine and oxime molecules the results also indicate an interaction *via* the P═O of DMMP. Finally TPD and interaction with water were also tested in this reactor and some useful aspects for the development of the sensors can be drawn from these results: the grafted molecules seem stable until 200 °C while DMMP can be removed thermally around 150 °C. In the case of TiO_2 some of the DMMP is removed by dissociative desorption involving surface hydroxide groups of oxide and leaving the P–CH_3 group attached to the oxide. Under vacuum conditions, the presence of water molecules preadsorbed on the sample limited DMMP absorption probably due to competitive formation of hydrogen bonds.

All these results achieved on TiO_2 powders open some paths for the regeneration to future sensors and need to be explored and confirmed in detail on nanostructured and functionalized microcantilevers towards real OP agents. Preliminary studies achieved under conditions closer to real usage indicate that the RH contained in air does not seem to prevent DMMP absorption on the nanostructure (Fig. S5, ESI†) and that our functionalized and nanostructured microcantilever has a lower frequency shift when exposed to high concentrations of acetone and ethanol than when exposed to low concentrations of DMMP (Fig. S6, ESI†). Future work will focus on advanced studies of these interactions and the use of light and heat to desorb faster the analyte for more rapid analysis.

Author contributions

Urelle Biapo: investigation, data curation, visualization, and writing – original draft. Valérie Keller: funding acquisition, conceptualization, and project administration. Philippe Bazin: investigation, Data curation, writing – original draft, and resources. Thomas Cottineau: supervision, visualization, investigation, writing – original draft, review & editing, and methodology.

Conflicts of interest

There are no conflicts to declare.

Acknowledgements

This work was financially supported by the ANR Bionanodetect project (ANR-15-CE39-0001). The authors would like to thank Thierry Dintzer and Dris Ihiawakrim for SEM and TEM images. We thank Vasiliki Papaefthymiou for the XPS measurements. Laurent Schlur and Denis Spitzer are gratefully acknowledged for their help with the resonating AFM experiment.

References

1 J. Kassa, *J. Toxicol., Clin. Toxicol.*, 2002, **40**, 803–816.
2 E. J. Mew, P. Padmanathan, F. Konradsen, M. Eddleston, S.-S. Chang, M. R. Phillips and D. Gunnell, *J. Affective Disord.*, 2017, **219**, 93–104.
3 Y. Sun and K. Y. Ong, *Detection Technologies for Chemical Warfare Agents and Toxic Vapors*, CRC Press, 2004.
4 Y. Seto, M. Kanamori-Kataoka, K. Tsuge, I. Ohsawa, K. Iura, T. Itoi, H. Sekiguchi, K. Matsushita, S. Yamashiro, Y. Sano, H. Sekiguchi, H. Maruko, Y. Takayama, R. Sekioka, A. Okumura, Y. Takada, H. Nagano, I. Waki, N. Ezawa, H. Tanimoto, S. Honjo, M. Fukano and H. Okada, *Anal. Chem.*, 2013, **85**, 2659–2666.
5 Y. Seto, M. Kanamori-Kataoka, K. Tsuge, I. Ohsawa, K. Matsushita, H. Sekiguchi, T. Itoi, K. Iura, Y. Sano and S. Yamashiro, *Sens. Actuators, B*, 2005, **108**, 193–197.
6 F. Arduini, A. Amine, D. Moscone, F. Ricci and G. Palleschi, *Anal. Bioanal. Chem.*, 2007, **388**, 1049–1057.
7 F. A. Harraz, *Sens. Actuators, B*, 2014, **202**, 897–912.
8 A. Boisen, S. Dohn, S. S. Keller, S. Schmid and M. Tenje, *Rep. Prog. Phys.*, 2011, **74**, 036101.
9 M. Alvarez and L. M. Lechuga, *Analyst*, 2010, **135**, 827–836.
10 R. K. Ahmad, A. C. Parada, S. Hudziak, A. Chaudhary and R. B. Jackman, *Appl. Phys. Lett.*, 2010, **97**, 093103.
11 L. Schlur, M. Hofer, A. Ahmad, K. Bonnot, M. Holz and D. Spitzer, *Sensors*, 2018, **18**, 1108.

12 J. Xu, A. Setiono and E. Peiner, *ACS Appl. Nano Mater.*, 2020, **3**, 6609–6620.
13 P. G. Datskos, N. V. Lavrik and M. J. Sepaniak, *Sens. Lett.*, 2003, **1**, 25–32.
14 L. A. Pinnaduwage, V. Boiadjiev, J. E. Hawk and T. Thundat, *Appl. Phys. Lett.*, 2003, **83**, 1471–1473.
15 S. Guo, P. Xu, H. Yu, X. Li and Z. Cheng, *Sens. Actuators, B*, 2015, **209**, 943–950.
16 D. Troya, A. C. Edwards and J. R. Morris, *J. Phys. Chem. C*, 2013, **117**, 14625–14634.
17 G. W. Wagner, P. W. Bartram, O. Koper and K. J. Klabunde, *J. Phys. Chem. B*, 1999, **103**, 3225–3228.
18 S. M. Kanan and C. P. Tripp, *Langmuir*, 2001, **17**, 2213–2218.
19 S. Cai, W. Li, P. Xu, X. Xia, H. Yu, S. Zhang and X. Li, *Analyst*, 2019, **144**, 3729–3735.
20 D. Spitzer, T. Cottineau, N. Piazzon, S. Josset, F. Schnell, S. N. Pronkin, E. R. Savinova and V. Keller, *Angew. Chem., Int. Ed.*, 2012, **51**, 5334–5338.
21 T. Cottineau, S. N. Pronkin, M. Acosta, C. Mény, D. Spitzer and V. Keller, *Sens. Actuators, B*, 2013, **182**, 489–497.
22 G. Thomas, G. Gerer, L. Schlur, F. Schnell, T. Cottineau, V. Keller and D. Spitzer, *Nanoscale*, 2020, **12**, 13338–13345.
23 U. Biapo, A. Ghisolfi, G. Gerer, D. Spitzer, V. Keller and T. Cottineau, *ACS Appl. Mater. Interfaces*, 2019, **11**, 35122–35131.
24 U. Biapo, A. Ghisolfi, G. Gerer, D. Spitzer, V. Keller and T. Cottineau, *IEEE Sensors*, IEEE, Montreal, QC, Canada, 2019, pp. 1–4.
25 J. Yang, M. Puchberger, R. Qian, C. Maurer and U. Schubert, *Eur. J. Inorg. Chem.*, 2012, 4294–4300.
26 V. V. Burungale, V. V. Satale, A. M. Teli, A. S. Kamble, J. H. Kim and P. S. Patil, *J. Alloys Compd.*, 2016, **656**, 491–499.
27 A. Kumar, A. R. Madaria and C. Zhou, *J. Phys. Chem. C*, 2010, **114**, 7787–7792.
28 D.-D. Qin, Y.-P. Bi, X.-J. Feng, W. Wang, G. D. Barber, T. Wang, Y.-M. Song, X.-Q. Lu and T. E. Mallouk, *Chem. Mater.*, 2015, **27**, 4180–4183.
29 H. Cheng, J. Ma, Z. Zhao and L. Qi, *Chem. Mater.*, 1995, **7**, 663–671.
30 T. Bezrodna, G. Puchkovska, V. Shymanovska, J. Baran and H. Ratajczak, *J. Mol. Struct.*, 2004, **700**, 175–181.
31 L. Mino, Á. Morales-García, S. T. Bromley and F. Illas, *Nanoscale*, 2021, **13**, 6577–6585.
32 L. Mino, C. Negri, R. Santalucia, G. Cerrato, G. Spoto and G. Martra, *Molecules*, 2020, **25**, 4605.
33 K. E. Lewis and G. D. Parfitt, *Trans. Faraday Soc.*, 1966, **62**, 204.
34 C. Pérez León, L. Kador, B. Peng and M. Thelakkat, *J. Phys. Chem. B*, 2006, **110**, 8723–8730.
35 M. Buchholz, M. Xu, H. Noei, P. Weidler, A. Nefedov, K. Fink, Y. Wang and C. Wöll, *Surf. Sci.*, 2016, **643**, 117–123.
36 Y.-G. Lei, K. ng, L. T. Weng, C.-M. Chan and L. Li, Surf. Interface Anal., *Surf. Interface Anal.*, 2003, **35**, 852–855.
37 G. A. Jeffrey, *An Introduction to Hydrogen Bonding*, Oxford University Press, Oxford, 1997.
38 F. Worek, H. Thiermann and T. Wille, *Arch. Toxicol.*, 2020, **94**, 2275–2292.
39 M. B. Mitchell, V. N. Sheinker and E. A. Mintz, *J. Phys. Chem. B*, 1997, **101**, 11192–11203.
40 A. R. Head, X. Tang, Z. Hicks, L. Wang, H. Bleuel, S. Holdren, L. Trotochaud, Y. Yu, L. Kyhl, O. Karslıoğlu, K. Fears, J. Owrutsky, M. Zachariah, K. H. Bowen and H. Bluhm, *Catal., Struct. React.*, 2017, **3**, 112–118.
41 J. Quenneville, R. S. Taylor and A. C. T. van Duin, *J. Phys. Chem. C*, 2010, **114**, 18894–18902.
42 V. M. Bermudez, *Langmuir*, 2010, **26**, 18144–18154.
43 O. M. Primera-Pedrozo, C. G. Fraga, A. Breton-Vega, M. M. Zumbach, B. P. Wilkins, N. S. Mirjankar and Z. C. Kennedy, *Forensic Chem.*, 2020, **20**, 100260.